Time-Dependent Simulation of a Semiconductor Laser Amplifier: Pulse Compression in a Ring Configuration and Dynamic Optical Bistability

MARTIN SCHELL AND ECKEHARD SCHÖLL

Abstract—**We present a dynamic theory of a semiconductor laser amplifier with time-dependent optical input signal and driving injection current. Previous treatments are extended by including a carrier density-dependent refractive index, a frequency-dependent gain, and multimode operation. The simulation yields optical bi- and tristability strongly depending upon the speed, at which the optical input–output characteristic is scanned. Tristability can be found in case of high pumping and large linewidth enhancement factor only.**

Applying our theory to a ring laser configuration we find asymptotic pulse compression, which can lead to the emission of a stable sequence of short pulses with widths down to about 6 ps. The face reflectivities, the external loss in the optical feedback loop, the detuning between the current repetition time and the optical round-trip time, the peak injection current, and the spectral linewidth of the gain are varied in order to check their influence on the optical pulsewidth. The shortest pulses are predicted for high optical feedback and low facet reflectivities. Even with reflectivities as low as 10^{-5} the pulsewidth is limited by the Fabry–Perot linewidth, rather than by the spectral gain linewidth.

I. Introduction

THE generation and amplification of short optical pulses by semiconductor laser amplifiers (SCLA's) is of great current interest [1]–[21] because of their potential applications in optical communication systems. Another important effect in SCLA's is provided by bistability in the optical input–output characteristic, which could be useful, for example, in digitizing optical pulses [24]–[32].

The production of short optical pulses by means of gain switching was treated earlier in a number of papers [2], [3], [5], [11]. In this paper we present a more general theoretical approach which allows us to deal with gain switching and with active mode locking in an external cavity to produce a sequence of (coherent) short pulses. In order to extend the analysis of single-pulse amplification [12] to the regime of active mode locking, we generalize the model used in [11] and [12] by including the frequency dependence of the gain, and the dependence of the refractive index upon carrier density.

Furthermore, the treatment of spontaneous emission is now included by adding a random electric field rather than by an additional rate equation for the photon density created by spontaneous emission. This introduces a direct coupling between spontaneous emission and the signal wave. We describe our novel simulation method and apply it to two different physical situations: 1) dynamic optical bistability (especially with rapidly varied optical input) and 2) active mode locking in a ring configuration. In the latter case a number of parameters are varied in order to determine the lower limit for the pulsewidth.

Manuscript received June 30, 1989; revised October 17, 1989.

M. Schell is with the Institut für Festkörperphysik, Technische Universität Berlin, D-1000 Berlin 12, West Germany.

E. Schöll is with the Institut für Theoretische Physik, Technische Universität Berlin, D-1000 Berlin 12, West Germany.

IEEE Log Number 9035218.

III. The Simulation Method

The electrons are described by the common rate equation [2], [4], [35]

$$\dot{n} = \eta J(t)/(ed) - \tilde{W}(n) - W(n)\bar{S} \qquad (1)$$

where n is the spatially averaged (over the SCLA's active region) carrier density, η is the injection efficiency, e is the elementary charge, d is the active layer thickness, $J(t)$ is the time-dependent injection current density, $\tilde{W}(n)$ is the rate of spontaneous emission, $W(n)$ is the modal gain, and $\bar{S}$ is the axially averaged photon density. In the following, $W(n) = g_0(n - n_0)$, with transparency concentration n_0 and modal gain constant g_0, and $\tilde{W}(n) = Bn^2$ are chosen, not for principal reasons, but for the sake of simplicity. Note that in contrast to our treatment of the electromagnetic field, which will be described below, here the spectral gain $g(\omega)$ is approximated by a constant g_0, and g_0 is chosen as the maximum of $g(\omega)$. This assumption is surely justified, because the spectral gain only varies about 0.2% in the occurring frequency band, which gives an appreciable effect in the mode competition, but not in the *integral* $\bar{S}$, which is the total intensity summed over all modes.

The electromagnetic field is described by a differential equation, which can be derived from the Maxwell equations with the common slowly varying amplitude and rotating wave approximations [8], [13],

$$\frac{\partial E^{\pm}}{\partial t} \pm v_g \frac{\partial E^{\pm}}{\partial z} = \frac{1}{2}\left\{\Gamma g(\omega)\left[(n - n_0) + i\alpha(n - n_t)\right] - \kappa'\right\}E^{\pm}. \qquad (2)$$

Here $E^{\pm}(t, z)$ is the complex amplitude of the forward–backward (in the z-direction) traveling electromagnetic field without the fast oscillating part $\sim \exp(i(\omega t \pm kz))$, $v_g = c/n_g$ is the group velocity, Γ is the optical confinement factor, $n_t = n_0 + (\kappa' - \ln(r_1 r_2)/\tau)/(\Gamma g_0)$ is the threshold carrier density, κ' is the optical loss inside the SCLA, and $\alpha \equiv -\chi_r'/\chi_i'$ with

$$\chi_r' = \left.\frac{\partial \operatorname{Re}(\chi(n))}{\partial n}\right|_{n=n_t}; \quad \chi_i' = \left.\frac{\partial \operatorname{Im}(\chi(n))}{\partial n}\right|_{n=n_t}$$

is the linewidth enhancement or antiguiding factor where χ is the complex dielectric susceptibility.

Our basic model is constituted by (1) and (2) supplemented by the boundary conditions

$$\begin{aligned} E^+(t, 0) &= r_1 E^-(t, 0) + t_1 E_{\text{in}}^+(t) \\ E^-(t, L) &= r_2 E^+(t, L) + t_2 E_{\text{in}}^-(t) \\ E_{\text{out}}^+(t) &= t_2 E^+(t, L) \\ E_{\text{out}}^-(t) &= t_1 E^-(t, 0) \end{aligned} \tag{3}$$

where r_1, r_2 and t_1, t_2 are the reflection and transmission coefficients, respectively, of the two facets, satisfying $r_i^2 + t_i^2 = 1$ and $r_i^2 = R_i$. $E_{\text{in}}^{\pm}(t)$ and $E_{\text{out}}^{\pm}(t)$ are the optical input and output field amplitudes (Fig. 1).

The time-dependent solutions are computed iteratively with the approximation that during sufficiently small, discrete timesteps Δt, the electric field is integrated with constant $n(t)$ and the carrier density is subsequently integrated with $\bar{S}(t)$. Rather than using a fixed discrete set of mode equations in the time domain, we Fourier-transform the fields during each timestep and amplify them in the frequency domain.

In our simulation we use the discretization scheme for (2) sketched in Fig. 1. Note that all fields are normalized to the dimension of $\text{cm}^{-3/2}$. During each timestep of length $\Delta t = \tau/N_{\text{ST}}$ (τ: single-pass time, N_{ST}: number of discrete points chosen) for the integration of (1) and (2) the following procedure is taken.

1) Simulation of Spontaneous Emission: An electrical field $E_{\text{SP}}^{\pm}(t, i)$ with $|E_{\text{SP}}^{\pm}(t, i)|^2 \sim \beta B n^2$, where β is the spontaneous emission factor, and a *random* phase is added at each of the $2N_{\text{ST}}$ points of Fig. 1.

2) Amplification with Frequency-Dependent Gain: The forward and backward traveling waves $E^+(t, i)$ and $E^-(t, i)$ corresponding to one cavity round-trip are Fourier-transformed according to

$$\tilde{E}\left(t, j\frac{\Delta\omega_{\text{FP}}}{N_{\text{ST}}}\right) := \sum_{k=1}^{N_{\text{ST}}} \left\{ E^+(t, k) \exp\left(-i\frac{kj\pi}{2N_{\text{ST}}}\right) + E^-(t, k) \exp\left(-i\frac{(k + N_{\text{ST}})j\pi}{2N_{\text{ST}}}\right)\right\}$$

$$j = (-N_{\text{ST}} + 1), \cdots, N_{\text{ST}}. \tag{4}$$

Thus $\tilde{E}(t, j\Delta\omega_{\text{FP}}/N_{\text{ST}})$ corresponds to the complex amplitude of the frequency part of the electrical field inside

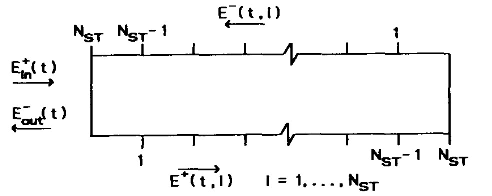

Fig. 1. Discretization scheme: traveling wave fields $E^{\pm}(t, z)$ are replaced by $E^{\pm}(t, i)$, $i \in \mathbb{N}$ with $z = \frac{1}{2}[L \pm (-L + i2L/N_{\text{ST}})]$; L is length of SCLA, which is divided into N_{ST} equal intervals.

the laser with the frequency $j\Delta\omega_{\text{FP}}/N_{\text{ST}}$, where $\Delta\omega_{\text{FP}} \equiv \pi/\tau$ is the spectral spacing of the SCLA's Fabry–Perot modes. $\tilde{E}$ is amplified with the following complex amplitude gain for one timestep:

$$G_{\Delta t}(\omega, n) = \exp\left\{\frac{1}{2}\left[\Gamma g_0\left(1 - \left(\frac{\omega - \omega_0}{\Delta\omega_g}\right)^2\right) \cdot ((n - n_0) + i\alpha(n - n_t)) - \kappa'\right]\tau/N_{\text{ST}}\right\}. \tag{5}$$

This is equivalent to an integration of (2) for the timestep Δt with the assumption that $n(t)$ does not vary during this time. Here the spectral gain function $g(\omega)$ is expanded around its maximum g_0, and $\Delta\omega_g = \sqrt{2g_0} \, |\partial^2 g(\omega)/\partial\omega^2|_{\omega=\omega_0}|^{-1/2}$ is a measure for the gain linewidth. Note that ω_0 is chosen as the carrier frequency of $E^{\pm}(t, z)$ and is supposed to be a Fabry–Perot resonance frequency for $\alpha = 0$. Inverse Fourier-transformation of $\tilde{E}$ leads to the amplified signal amplitudes $E^{\pm}(t + \Delta t, i + 1)$, $i = 1, \cdots, N_{\text{ST}} - 1$. For $i = N_{\text{ST}}$, additionally, the boundary conditions (3) are necessary.

3) Integration of the Carrier Rate Equation: Equation (1) is integrated using a Runge–Kutta scheme. Here, $\bar{S}$ is computed according to

$$\bar{S}(t) = \frac{1}{2N_{\text{ST}}} \sum_{i=1}^{N_{\text{ST}}} \left(|E^+(t, i)|^2 + |E^-(t, i)|^2\right). \tag{6}$$

4) Input and Output: The optical input and output field amplitudes $E_{\text{in}}^{\pm}(t)$ and $E_{\text{out}}^{\pm}(t)$ are included via the boundary conditions (3).

This model takes account of multiple reflections and interference of the traveling waves, a carrier-density dependent refractive index (linewidth enhancement factor, associated with frequency chirp), frequency-dependent gain, and spontaneous emission in a simulated frequency band of the width $\pm N_{\text{ST}}\Delta\omega_{\text{FP}}$. The frequency resolution, which is only limited by the total simulation time and the computer resources, was typically 1 GHz.

We have not included in our simulation spectral or spatial hole burning effects, gain saturation [$\bar{S}$-dependence of $W(n)$] and, due to the plane-wave approximation, optical modes higher than TEM_{00}.

III. Optical Bistability

Bistability in the optical input–output characteristic is of current interest in view of its possible applications in optical computing or digitizing of optical pulses [24]–[32]. Here the laser is driven by a CW injection current, while an optical input signal is coupled in at one side of the SCLA (Fig. 2). Due to the plane-wave approximation spatial instabilities, which also produce interesting time-dependent behavior, cannot be included at this level of desription (for a review on these phenomena see [34]).

While many authors have treated the static theory [24]–[26], the time-dependent behavior below the threshold has been analyzed in [28]–[32]. One aim of this paper is to develop a novel integration method which is so general that it is appropriate for both optical bistability and active mode locking, and apply it to dynamic optical bistability above threshold.

Note that the simulations in this paper are performed without gain saturation which is not necessary for understanding optical bistability or *active* mode locking. Inclusion of gain saturation ($\bar{S}$-dependence of g_0) could be a useful further extension of the theory.

In the following simulations the optical input was chosen in a triangular form (for the case of simplicity) (Fig. 3) where t_C is the sweeping time of the input–output characteristic. As our method allows for any arbitrary time dependence of the input there would be no problem to extend our simulations to more realistic input shapes. The other parameters used in the simulations of this paper are listed in Table I.

Although the simulated optical input signal was only slowly varying on the scale of the single-pass time the simulations have shown that the number of discretization points must be at least $N_{ST} = 2$ to provide satisfactory agreement with the static theory in the case of long t_C. This is caused by the exponential growth of the backward and forward traveling field intensities inside the SCLA leading to a spatial inhomogeneity in $|E^+|^2 + |E^-|^2$. Note that N_{ST} simultaneously determines the temporal and spatial resolution.

A particular choice of the center frequency ω_{in} of $E_{in}(t)$ only shifts the regions of bistability on the $|E_{in}|^2$-axis and is chosen as $\omega_{in} = \omega_0 + \omega'_{in}\Delta\omega_{FP}$, where ω_0 is the frequency of maximum spectral gain and $\omega'_{in} = 0.25$ determines the optical input frequency.

Fig. 4(a) shows a simulation in the quasistatic regime ($t_C = 33$ ns, full line) in comparison with a static analytical solution (dotted line) calculated from the active Fabry–Perot theory [9], [11]:

$$|E_{out}|^2 = \frac{(1 - r_1^2)(1 - r_2^2)G_s}{(1 - r_1 r_2 G_s)^2 + 4 r_1 r_2 G_s \sin^2(\varphi)} |E_{in}|^2 \quad (7)$$

with

$$\varphi = \pi\omega'_{in} + \frac{\alpha}{2}\tau\Gamma g_0(n - n_t),$$

$$G_s = \exp\left((\Gamma g_0(n - n_0) - \kappa')/\tau\right) \quad (8)$$

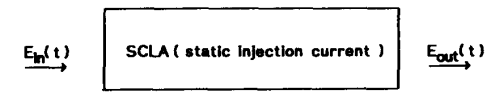

Fig. 2. Configuration used for simulation of optical bistability.

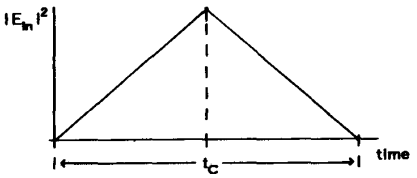

Fig. 3. Optical input as function of time used for simulation of optical bistability.

TABLE I
Parameters for the Simulations[a]

B	$1.6 \cdot 10^{-10}$ cm³/s
g_0	$4 \cdot 10^{-6}$ cm³/s
κ'	$0.722 \cdot 10^{12}$/s
β	10^{-4}
Γ	0.2
n_0	$1.25 \cdot 10^{18}$ cm^{-3}
$\Delta\omega_{FP}$	$2\pi \cdot 125$ GHz
$\Delta\omega_g$	$40 \cdot \Delta\omega_{FP}$
L	300 μm
$R_{1,2}$	$r_1^2 = r_2^2 = 0.33$
n_B	4
T_J	1024 ps
T_E	1024 ps
N_{ST}	2
λ_0	0.8 μm
ω_0	$2\pi c/\lambda_0$

[a]Parameters are shown for the simulations (unless listed differently in the respective figure caption).

where n is determined from a self-consistent solution of (1) in the steady state with $\bar{S} = N + \bar{S}'$, together with the equations for the photon densities of amplified spontaneous emission N and amplified signal $\bar{S}'$ [11]:

$$0 = \Gamma g_0(n - n_t)N + \beta B n^2$$

$$\bar{S}' = \frac{1}{t_2^2}\frac{(|G_s| - 1)(1 + r_2^2|G_s|)}{|G_s| \ln |G_s|}|E_{out}|^2.$$

The electrical field intensities are plotted in units of the threshold carrier density n_t. The simulation displays a short relaxation oscillation when changing from one stable state to the other. This oscillation is reduced gradually with decreasing sweeping speed, but does not fully disappear. The intensity spike in the up-switch has also been found in experiments [29] and other simulations [28], [29], [31], [32] and is a general phenomenon in dispersive optical bistability, related to passing through a Fabry–Perot resonance. The spike in the down-switch can occur only if the laser is operated above threshold where the lowest output branch corresponds already to a lasing state.

The differences between the static theory and the time-dependent simulations in the high-power input region can

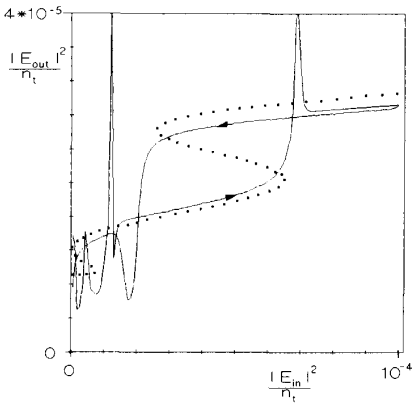

(a)

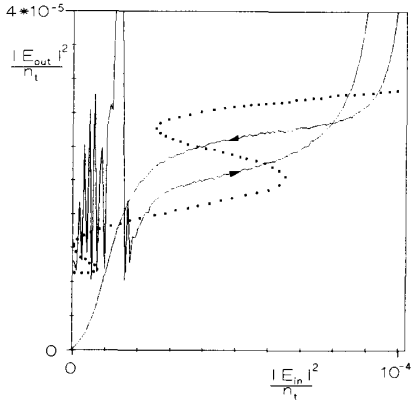

(b)

Fig. 4. Optical bistability: normalized optical output intensity is plotted versus optical input intensity for $J = 1.2\ J_t$ (J_t threshold current density), $\omega_{in}' = 0.25$, $\alpha = 7$, and (a) $t_C = 33$ ns and (b) $t_C = 4$ ns. (Full line: time-dependent numerical solution, dotted line: static analytical solution.)

be explained by a linearization of the bimolecular rate of spontaneous emission, which is necessary in the analytic solution. Another difference with respect to the static theory can be seen in the oscillatory behavior for low, increasing optical input intensity. The oscillations are due to oscillations in the carrier density. They appear to be related to the usual relaxation oscillations occurring above laser-threshold. We note that—in contrast to other simulations [28]–[32]—we bias the laser with an injection current *above* threshold.

Fig. 4(b) shows the switching characteristics for a value of $t_C = 4$ ns. The occurrence of optical bistability is obviously confined to slowly varying optical input. Here "slowly" means slowly on the scale of the carrier recombination time, because the switching between different output branches is connected with a change in carrier density [33]. The sweeping-speed dependence of the input–output characteristics is in qualitative agreement with measured hysteresis curves [29] though a sinusoidal (rather than a triangular) input intensity was used there.

Multistable behavior with more than two stable output intensities corresponding to one input intensity is limited to the high pumping, high input, and long t_C-regime. Fig. 5 shows a typical simulation of tristability. The middle one of the three stable branches (AB) is only reached if the SCLA is *not* driven to input intensities large enough to switch to the highest possible output branch.

IV. Active Mode Locking in Ring Configurations

Active mode locking in SCLA's requires an external cavity due to the short round-trip time, which leads to a high Fabry–Perot-mode difference frequency, which is above the limit for electrical pulse-generators. The scheme for the simulated configuration is shown in Fig. 6(a). The pumping current is chosen as a Gaussian [Fig. 6(b)] with maximum J_{max}, repeated every $T_J = 1024$ ps. The external cavity is assumed to have a linear dispersion, so that

$$E_{in}^{\pm}(t) = r_{ext} E_{out}^{\pm}\left(t - (T_E - \tau)\right)$$

with

$$r_{ext} = R_{ext}^{1/2};\ R_{ext} \in \mathbb{R}^+$$

holds (with T_E the total roundtrip time and R_{ext} the relative intensity loss in the external cavity). A theoretical treatment of mode locking a SCLA in an external (linear) cavity has been given in [22] and [23], for example. Their analytical solutions are restricted to a sinusoidal time dependence of the gain (no gain depletion) and do not include, for example, the back reflection at the laser facets into the cavity, the carrier density dependence of the refractive index, or the spontaneous emission.

With the help of our simulations we shall address the following questions:

- What is the lower limit for the pulse FWHM (full width at half maximum), and is it determined by the SCLA Fabry–Perot linewidth or rather by the spectral gain linewidth?
- What is the influence of the α parameter (frequency chirp)?
- What is the influence of spontaneous emission?
- What is the effect of cavity detuning ($T_E \neq T_J$)?
- What is the limit for the injection current to be applied?

First, in Fig. 7(a), (b), and (c) we show the power spectrum, the temporal evolution of the output intensities, and the carrier density of every fifth emitted pulse for zero optical feedback, respectively, i.e., when gain switching is the mechanism leading to the short pulses. The maximum of the injection current J_{max} is optimized such that the shortest pulses are produced under the constraint that subsequent relaxation oscillations are suppressed.

The substructure of subsequent emitted pulses results from the interference of different Fabry–Perot modes. Due to the statistical nature of spontaneous emission and the absence of feedback, the SCLA "forgets" the phases of the different Fabry–Perot modes between two pulses, which leads to missing spectral correlation [Fig. 7(a)] and to an erratic change in the substructure between subse-

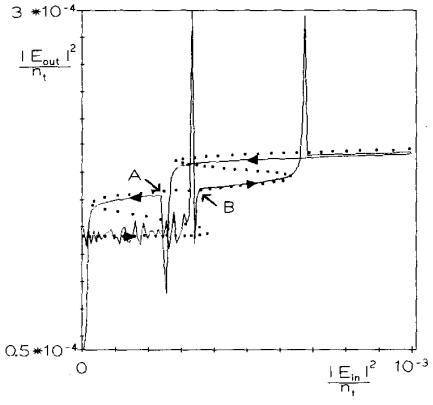

Fig. 5. Optical tristability, plotted as in Fig. 4, with $J = 4J_t$, $\omega'_{in} = -0.5$, $\alpha = 7$, $t_C = 16$ ns, and maximum $|E_{in}|^2 = 10^{-3}\, n_t$.

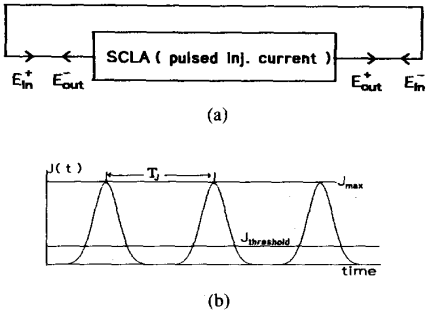

Fig. 6. (a) Scheme of ring configuration. (b) Injection current versus time.

quent pulses [Fig. 7(b)]. The gain depletion causes a sharp cutback in carrier density [Fig. 7(c)] during the pulse emission. This step leads to a widening of the SCLA Fabry–Perot-modes [Fig. 7(d)], when additionally the carrier dependence of the refractive index ($\alpha = 3$ instead of $\alpha = 0$) is introduced. The spectral "rabbit ears" in Fig. 7(d) are also found experimentally [16]. The pulsewidth is not affected by a nonzero α. Note that the asymptotic pulse FWHM averaged over the last 20 pulses is 13 ps, which is the optimum to be reached with this configuration, with the given pumping pulse reptition time T_J and *without* feedback. With increasing T_J the pulsewidth slightly decreases.

A. Low Feedback and High Reflectivities

Fig. 8(a) and (b) shows the shortest possible pulses obtained with the same parameters as in Fig. 7(a)–(c), but with an external feedback rate of $R_{ext} = 10\%$ and an appropriately lowered maximum of the injection current. The FWHM (12 ps) is slightly less than in Fig. 7 and the spectra exhibit a certain amount of correlation between subsequent pulses. The fine structure of subsequent pulses [Fig. 8(b)] is more stable than in Fig. 7(b), but small variations for subsequent k_T indicate that mode locking is not yet complete. This result prompts one to attempt to produce still shorter and more coherent pulses by further increasing R_{ext}.

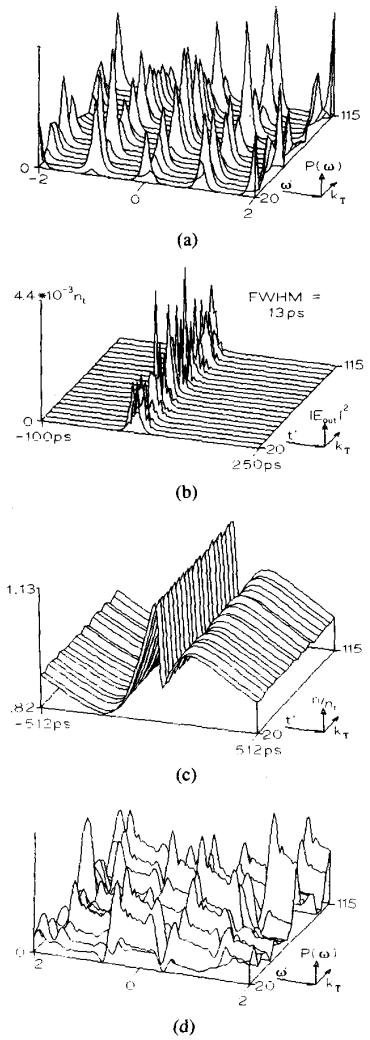

Fig. 7. Simulation for periodic injection current *without* feedback. ($J_{max} = 6.1\, J_t$, $\alpha = 0$, $\omega' = (\omega - \omega_0)/\Delta\omega_{FP}$ is normalized frequency, $k_T \in \mathbb{N}$ is index that labels subsequent emitted pulses, t' is time scale for one pulse with total elapsed time $t = k_T T_J + t'$, and $-T_J/2 < t' \le T_J/2$.)
(a) Power spectrum of output field

$$P(\omega', k_T) \sim \left| \int_{(k_T - 1/2)T_J}^{(k_T + 1/2)T_J} E^+_{out}(t) \exp\left(-i(\omega_0 + \omega' \Delta\omega_{FP})t\right) dt \right|^2.$$

(b) Temporal evolution of normalized output intensity

$$|E_{out}(t', k_T)|^2 = |E^+_{out}(t - k_T T_J)|^2.$$

(c) Carrier density n/n_t. (d) Influence of linewidth enhancement factor in the gain-switching regime (same plot as in (a), but with $\alpha = 3$ instead of $\alpha = 0$).

B. High Feedback and High Reflectivities

Fig. 9 with $R_{ext} = 50\%$ shows that the situation is, however, more complicated: Although there is complete coherence and form stability between subsequent pulses, the FWHM has drastically increased. The reason lies in

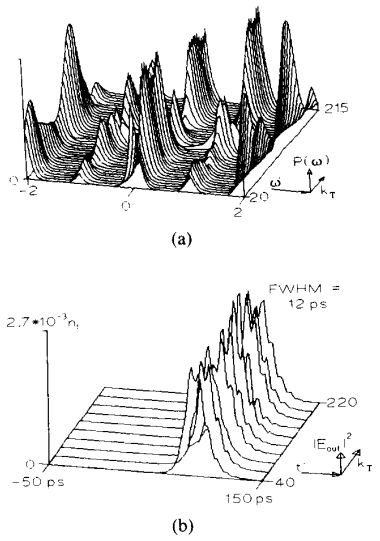

Fig. 8. Simulation of ring configuration with low feedback and high reflectivities (same parameters as in Fig. 7(a)-(c), but $R_{ext} = 0.1$ and lower maximum injection current ($J_{max} = 4.5\,J_t$) in accordance with decreased effective dynamic threshold). (a) Power spectrum of output field. (b) Temporal evolution of output intensity.

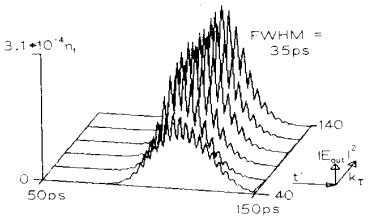

Fig. 9. Simulation of ring configuration with high feedback and high reflectivities (same parameters as in Fig. 8(b), but $R_{ext} = 0.5$, $J_{max} = 2.4\,J_t$).

the SCLA facet reflectivities, which lead to a strong Fabry–Perot-type behavior of the SCLA and to a relatively large amount of reflected optical input, which puts the system off phase after the next round-trip.

C. High Feedback and Low Reflectivities

The effects of reducing the SCLA facet reflectivities down to 0.01 (instead of $R_1 = R_2 = 0.33$) are shown in Fig. 10(a) and (b). The FWHM (21 ps) has decreased again, but is still larger than in the zero-feedback gain-switching regime. When $\alpha \neq 0$ is introduced now [Fig. 10(c)] the small variation of carrier density during the pulse's emission does not lead to a widening of the Fabry–Perot modes but to a frequency shift due to the lowered effective laser threshold.

The effect of a further reduction of the reflectivities is shown in Fig. 11. For values of about 10^{-3} the same FWHM as in the gain-switching case can be achieved. The extremely small value of 10^{-5} leads to a FWHM of about 6 ps. At this point again, a comment on the numerical resolution is in order. N_{ST} was chosen equal to 2 leading to a time step length of 2 ps. Although a higher resolution might be thought to be necessary to properly account for 6 ps pulses, tests with $N_{ST} = 4$ resulted in only slightly different FWHM. From further numerical checks we could exclude that the lower bound of the simulated pulse length was limited by the low numerical resolution. Also, the product of the pulse FWHM and the spectral bandwidth is at least by a factor 2 higher than for

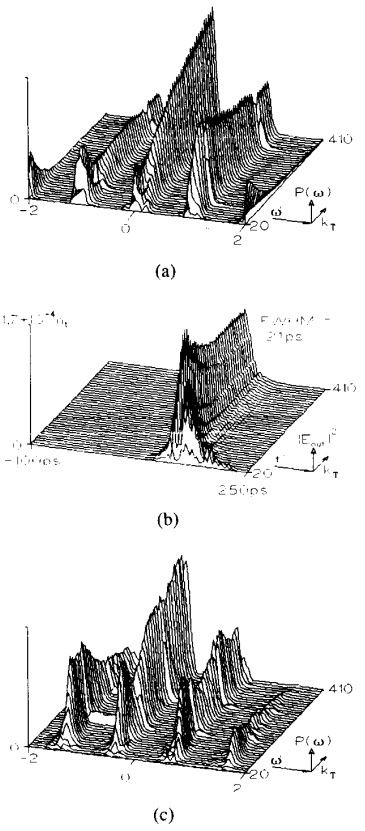

Fig. 10. Simulation of ring configuration with low feedback and low reflectivities (same parameters as in Fig. 9, but with $R_{1,2} = 0.01$, $J_{max} = 1.35\,J_t = 2.8\,J_{0.33}$, where $J_{0.33}$ is the injection current threshold for reflectivities of 0.33). (a) Power spectrum. (b) Temporal evolution of the output intensity. (c) Influence of the linewidth enhancement factor in mode-locking regime (same plot as in (a), but with $\alpha = 3$ instead of $\alpha = 0$).

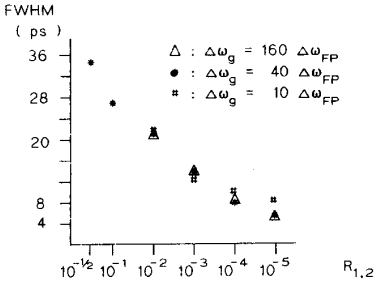

Fig. 11. Pulsewidth versus reflectivities for different gain linewidths $\Delta\omega_g$ ($\alpha = 0$, $R_{ext} = 0.5$, $J_{max} = 0.54\,J_t = 2.8\,J_{0.33}$).

a Gaussian (0.88), so that the pulsewidth is not Fourier-transform limited.

It remains as a question, whether 6 ps are a lower limit imposed by the spectral gain linewidth $\Delta\omega_g$. A repetition of the simulations with a spectral linewidth increased or decreased by a factor of 4 shows that only for $R = 10^{-5}$ there is a small broadening in the pulsewidth with decreasing gain linewidth. Also, a lowering of the spontaneous emission coefficient β by a factor of 10 effects a reduction of the FWHM by only 10%. This indicates that the Fabry-Perot character of the external-cavity/SCLA system mainly determines the lower limit of the FWHM for short pulse production by active mode locking (besides spontaneous emission).

The dynamics of short pulse production by active mode locking is shown in Fig. 12. Obviously the establishment of a fixed phase relation between the external cavity modes, which leads to the desired short pulses, is a continuous process which needs about 300–400 round trips to converge to the final asymptotic state.

D. Detuning

The introduction of a small amount of detuning ($T_E = T_J \pm 2$ ps $\triangleq 0.4\%$) leads to incoherent pulses, to slight temporal fluctuations in the carrier density, and to a large increase in the pulse FWHM ($T_E = T_J$: FWHM = 21 ps, Fig. 10; $T_E = T_J + 2$ ps: FWHM = 37 ps; $T_E = T_J - 2$ ps: FWHM = 39 ps). This change is significantly higher than expected from the analysis of [23].

E. Pumping Current

In the gain-switching regime an increase of the injection current intensity (with fixed width of the Gaussians) leads to still shorter pulses, but also to the onset of undesired further relaxation oscillations. Mode locking, however, which occurs for significantly lower injection intensities, is affected in the following way: the increased injection current leads to increased optical pulse intensities and thus to higher gain (and carrier) depletion during the emission of the pulse. Under the assumption that the ring configuration still behaves completely periodically (with period T_J) the increase of the carrier depletion is equivalent to an increase of higher order Fourier components in the temporal gain function. They are not included in the analytical solutions of [22] and [23], and lead to coupling between nonadjacent external modes. This coupling is then (and only then) in phase with the direct coupling when the gain is symmetric with respect to an arbitrary, but fixed time. As can be seen from the carrier density behavior in the gain-switching regime (Fig. 7) this symmetry does not exist. Hence the gain-depletion leads to a destruction of the mode-coupling mechanism as shown in Fig. 13, which was simulated with an injection current increased by 65% compared to the optimum (shortest possible pulses) current and leads to drastically broadened pulses. In contrast to that a raised injection current together with a "belated" ($T_E = T_J + 2$ ps) feedback causes a drastically reduced pulse width (FWHM = 12 ps). Here a direct transition to the gain switching regime occurs, because the "belated" preceding pulse depletes the carrier density after the emission of the present one and thus allows to use a higher injection current without inducing further relaxation oscillations.

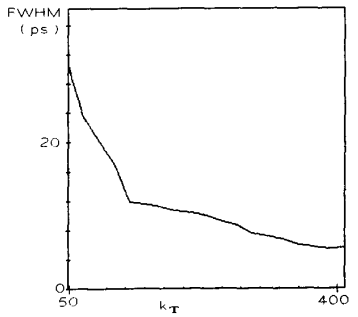

Fig. 12. Dynamics of pulse-compression: FWHM of output intensity is plotted versus index k_T that labels subsequent pulses, corresponding to number of round trips in ring configuration ($\alpha = 0$, $R_{ext} = 0.5$, $J_{max} = 0.54\, J_t = 2.8\, J_{0.33}$, $R_{1,2} = 10^{-5}$).

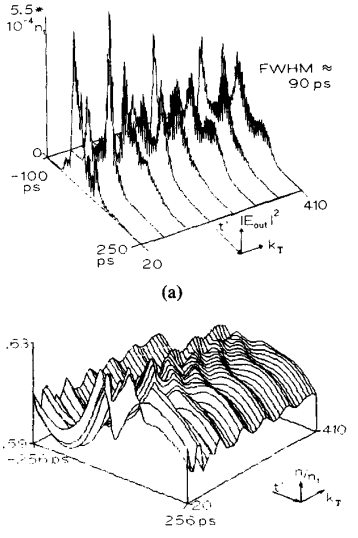

Fig. 13. Effect of too high an injection current ($T_E = T_J = 512$ ps, $R_{1,2} = 0.01$, $\alpha = 0$, $R_{ext} = 0.5$, $J_{max} = 1.3\, J_t = 2.7\, J_{0.33}$). The shortest pulses with FWHM = 20.8 ps were obtained for $J_{max} = 0.8\, J_t$. (a) Temporal evolution of the output intensity. (b) Carrier density.

V. Conclusion

The proposed novel simulation method is appropriate to treat a semiconductor laser amplifier with still reasonable computing effort for both time dependent optical input and time dependent injection current while including the carrier density dependence of the refractive index, the frequency dependence of the gain, and correct phase relationships of multiple reflections and optical input. Our method is applied to a linear configuration and to a ring configuration.

Our simulations of bi- or multistability in the optical input–output characteristic have revealed a strong dependence on the sweeping speed of the optical input which limits the switching speed to the timescale set by the carrier recombination time. Optical multistability was only found for high injection current, high input, and an α-parameter of the order of 7. Additionally, the fan out of the multistable simulations in the regime above the laser threshold was always significantly lower than unity (i.e., input power always greater than output power) which will strongly limit possible applications.

In ring configurations the production of short pulses by active mode locking appears to be mainly limited by the Fabry–Perot character of the system and not by the gain linewidth.

From the variation of various parameters (α, T_E, $J_{\max}$, $R_{1,2}$, R_{ext}) we obtain the prediction that the shortest pulses of about 6 ps can be obtained for a high optical feedback and very low facet reflectivities. This seems to be a general limit for active mode locking, and is also found experimentally [17], [18].

Even for facet reflectivities down to 10^{-5} the gain linewidth limit for the FWHM (~ 1 ps) cannot be reached. This indicates that locking of two external modes lying in different laser modes by active mode locking is either impossible, or would require still lower facet reflectivities.

Recently subpicosecond pulses were found by active mode locking by Corzine *et al.* [20]. Their work, however, is not directly comparable as they observed the subpicosecond pulses only for modulation with multiples of the external mode spacing frequency. It might also be conceivable that a very small amount of saturable absorption combined with the high modulation frequencies leads to the short pulses observed.

The injection current must be optimized individually in each case. Too high injection currents lead to the onset of relaxation oscillations in the gain-switching regime. Too high injection currents in the mode-locking regime, or too low currents in both regimes, lead to broadened pulses. The pulsewidth, however, is two or three orders of magnitude less sensitive to changes in the injection current than in [21], where a change of 1.5% in the injection current increases the pulsewidth by 800% for pulsed injection current.

A detuning between optical round-trip time T_E and pumping period T_J leads to less coupling between the external modes and thus to an increase in the pulse FWHM, which is significantly larger than in the analytical approximation [23]. The decrease of the FWHM predicted by Demokan [21] for detuning frequencies of about 500 kHz was not analyzed as our lowest detuning frequency was 8 MHz. In the gain-switching regime a "belated" feedback suppresses further relaxation oscillations and thus allows for higher injection current and slightly shorter pulses.

The carrier dependence of the refractive index (α parameter) leads to a broadening (in the gain-switching regime) or a shift (in the mode-locking regime) of the SCLA spectrum. We could not find significant effects of this upon the pulsewidth or the mode-locking properties, in agreement with experimental results [18].

The influence of spontaneous emission on the pulsewidth is very small. For 20 ps pulses, for example, a reduction or increase of the spontaneous emission factor by a factor of ten does not effect a visible change in the FWHM. For 6 ps pulses the same variation causes a change in FWHM of about 10%. This is again in contrast to [21].

Acknowledgment

The authors are grateful to D. Bimberg, E. H. Böttcher, R. Müller, K. A. Shore, and A. G. Weber for helpful discussions.

References

[1] J. P. van der Ziel, W. T. Tsang, R. A. Logan, R. M. Mikulayak, and W. M. Augustyniak, "Subpicosecond pulses from passively modelocked GaAs buried optical guide semiconductor lasers," *Appl. Phys. Lett.*, vol. 39, pp. 525–527, 1981.

[2] E. Schöll, D. Bimberg, H. Schumacher, and P. T. Landsberg, "Kinetics of ps-pulse generation in semiconductor lasers with bimolecular recombination at high current injection," *IEEE J. Quantum Electron.*, vol. QE-20, pp. 394–399, Apr. 1984.

[3] M. Osiński and M. J. Adams, "Picosecond pulse analysis of gain-switched 1.55 μm InGaAsP lasers," *IEEE J. Quantum Electron.*, vol. QE-21, pp. 1929–1936, Dec. 1985.

[4] K. Y. Lau and A. Yariv, "High-frequency current modulation of semiconductor injection lasers," in *Semiconductors and Semimetals*, vol. 22B, W. T. Tsang, Ed. Orlando, FL: Academic, 1985, pp. 70–152.

[5] D. Bimberg, K. Ketterer, E. H. Böttcher, and E. Schöll, "Gain modulation of unbiased semiconductor lasers: Ultrashort light-pulse generation in the .8 μm–1.3 μm wavelength range," *Int. J. Electron.*, vol. 60, pp. 23–45, 1986.

[6] M. Ikeda, "Switching characteristics of a laser diode switch," *IEEE J. Quantum Electron.*, vol. QE-19, pp. 157–163, 1983.

[7] T. Mukai, Y. Yamamoto, and T. Kimura, "Optical amplification by semiconductor lasers," in *Semiconductors and Semimetals*, vol. 22E, W. T. Tsang, Ed. Orlando, FL: Academic, 1985, pp. 265–319.

[8] D. Marcuse, "Computer model of an injection laser amplifier," *IEEE J. Quantum Electron.*, vol. QE-19, pp. 63–73, 1983.

[9] M. J. Adams, J. V. Collins, and I. D. Henning, "Analysis of semiconductor laser optical amplifiers," *Proc. Inst. Elect. Eng.*, vol. 132, pp. 58–63, 1985.

[10] I. D. Henning, M. J. Adams, and J. V. Collins, "Performance predictions from a new optical amplifier model," *IEEE J. Quantum Electron.*, vol. QE-21, pp. 609–613, June 1985; ——, *IEEE J. Quantum Electron.*, vol. QE-21, p. 1973, Dec. 1985.

[11] E. Schöll, "Dynamic theory of picosecond optical pulse-shaping by gain-switched semiconductor laser amplifiers," *IEEE J. Quantum Electron.*, vol. 24, pp. 435–442, Feb. 1988.

[12] E. Schöll and M. Schell, "Theory of ultrashort pulse generation and amplification by gain-switched laser amplifiers," *Physica Status Solidi (b)*, vol. 150, no. 2, pp. 575–579, 1988.

[13] R. Müller, "Amplitude and frequency modulation of light pulses in semiconductor Fabry–Perot amplifiers," *Physica Status Solidi (b)*, vol. 150, no. 2, p. 587–592, 1988.

[14] A. J. Lowery, "Explanation and modelling of pulse compression and broadening in travelling-wave laser amplifiers," *Electron. Lett.*, vol. 24, pp. 1125–1126, 1988.

[15] K. Ketterer, E. H. Böttcher, and D. Bimberg, "Picosecond spectra of gain-switched AlGaAs/GaAs multiple quantum well lasers," *Appl. Phys. Lett.*, vol. 53, pp. 2263–2266, 1988.

[16] H. Ishikawa, K. Kamite, K. Kihara, H. Sudo, M. Sugano, and H. Imai, "Evaluation of single mode property of DFB-Lasers by gain switched ultra short pulse operation," in *Proc. 11th IEEE Int. Semicond. Laser Conf.*, Boston, MA, 1988, paper G-5.

[17] G. Eisenstein, R. Tucker, U. Koren, and S. Korotky, "Active mode-locking characteristics of InGaAsP single mode fiber composite cavity lasers," *IEEE J. Quantum Electron.*, vol. QE-22, pp. 142–147, 1986.

[18] J. Kuhl, M. Serényi, and E. O. Göbel, "Bandwidth-limited picosecond pulse generation in an actively mode-locked GaAs laser with intracavity chirp compensation," *Opt. Lett.*, vol. 12, pp. 334–339, 1987.
[19] D. Baums, M. Serényi, W. Elsässer, and E. O. Göbel, "Instabilities in the power spectrum of mode-locked semiconductor lasers," *J. de Physique*, vol. 6, pp. C2/405–C2/408, 1988.
[20] S. W. Corzine, J. E. Bowers, G. Przybylek, U. Koren, B. I. Miller and C. E. Soccolich, "Actively mode-locked GaInAsP laser with subpicosecond output," *Appl. Phys. Lett.*, vol. 52, pp. 348–350, 1988.
[21] M. S. Demokan, "A model of a diode laser actively mode-locked by gain modulation," *Int. J. Electron.*, vol. 60, pp. 67–85, 1986.
[22] H. A. Haus, "Theory of mode-locking of a laser diode in an external resonator," *J. Appl. Phys.*, vol. 51, pp. 4042–4049, 1980.
[23] J. A. Yeung, "Theory of active mode-locking of a semiconductor laser in an external cavity," *IEEE J. Quantum Electron.*, vol. QE-17, pp. 399–404, 1981.
[24] M. J. Adams, H. J. Westlake, M. J. O'Mahony, and I. D. Henning, "A comparison of active and passive optical bistability in semiconductors," *IEEE J. Quantum Electron.*, vol. QE-21, pp. 1498–1504, 1985.
[25] H. Kawaguchi, K. Inoue, T. Matsuoka, and K. Otsuka, "Bistable output characteristics in semiconductor laser injection locking," *IEEE J. Quantum Electron.*, vol. QE-21, pp. 1314–1317, 1985.
[26] H. Kawaguchi, "Multiple bistability and multistability in a Fabry-Perot laser diode amplifier," *IEEE J. Quantum Electron.*, vol. QE-23, pp. 1429–1433, 1987.
[27] M. J. Adams, H. J. Westlake, and M. J. O'Mahony, "Optical Bistability in Semiconductor Laser Amplifiers," in *Optical Nonlinearities and Instabilities in Semiconductors*, H. Haug, Ed. Orlando, FL: Academic, p. 373, 1988.
[28] M. J. Adams, "Time dependent analysis of active and passive optical bistability in semiconductors," *IEE Proc., Pt. J*, vol. 132, pp. 343–348, 1985.
[29] H. J. Westlake, M. J. Adams, and M. J. O'Mahony, "Assessment of switching speed of optical bistability in semiconductor laser amplifiers," *Electron. Lett.*, vol. 22, no. 10, pp. 541–543, 1986.
[30] N. Ogasawara and R. Ito, "Static and dynamic properties of nonlinear semiconductor laser amplifiers," *Japan. J. Appl. Phys.*, vol. 25, pp. L739–L742, 1986.
[31] W. F. Sharfin and M. Dagenais, "Dynamics of optically switched bistable diode laser amplifiers," *IEEE J. Quantum Electron.*, vol. QE-23, pp. 303–308, 1987.
[32] A. J. Lowery, "New inline wideband dynamic semiconductor laser amplifier model," *IEE Proc., Pt. J*, vol. 135, pp. 242–250, 1988.
[33] M. J. O'Mahony, "Semiconductor laser optical amplifiers for use in future fiber systems," *J. Lightwave Technol.*, vol. 6, pp. 531–544, 1988.
[34] K. A. Shore and T. Rozzi, "Instabilities in Semiconductor Lasers," in *Optical Nonlinearities and Instabilities in Semiconductors*, H. Haug, Ed. Orlando, FL: Academic, p. 147, 1988.
[35] H. Haug, "Quantum mechanical rate equations for semiconductor lasers," *Phys. Rev.*, vol. 184, no. 2, pp. 338, 1989.

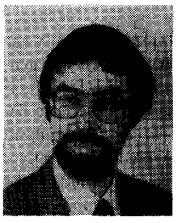

Eckehard Schöll was born in Stuttgart, West Germany, on Feburary 6, 1951. He received the Diplom degree in physics from the University of Tübingen, West Germany, in 1976, the Ph.D. degree in applied mathematics from the University of Southampton, England, in 1978, and the Dr.rer.nat. degree and the venia legendi (Habilitation) from the Institute of Theoretical Physics, Aachen University of Technology (RWTH), West Germany, in 1981 and 1986, respectively.

During 1983–1984 he was a Visiting Assistant Professor with the Department of Electrical and Computer Engineering, Wayne State University, Detroit, MI. During shorter visits, he was with the University of Florida, Gainesville and the University of Tübingen. Since 1989 he has been a professor of Theoretical Physics at the Technical University of Berlin. His research interests include the theory of nonlinear charge transport and current instabilities in semiconductors, nonlinear dynamics and chaos, and semiconductor laser theory.

Dr. Schöll is the author of approximately 50 research papers and the book on *Nonequilibrium Phase Transitions in Semiconductors*. He was the organizer of an international symposium on "Statistical Physics and Semiconductors," in 1987. He is a member of the Germany Physical Society.

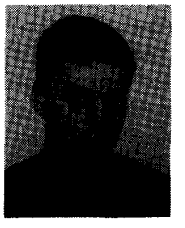

Martin Schell was born in Stuttgart, West Germany, on July 7, 1963. He received the diploma degree in August 1989 from the Rheinisch-Westfälische Technische Hochschule, Aachen, West Germany.

Besides actively mode-locking with semi-conductor lasers, he is presently engaged in research on DFB/DBR lasers, especially concerning the dynamic spectral behavior.